Accepted Manuscript

Improved microwave dielectric properties of $CaMgSi_2O_6$ ceramics through CuO doping

Yuanming Lai, Hua Su, Gang Wang, Xiaoli Tang, Xiaofeng Liang, Xin Huang, Yuanxun Li, Huaiwu Zhang, Chen Ye, X. Renshaw Wang

PII: S0925-8388(18)33297-3

DOI: 10.1016/j.jallcom.2018.09.059

Reference: JALCOM 47478

To appear in: *Journal of Alloys and Compounds*

Received Date: 9 June 2018

Revised Date: 3 September 2018

Accepted Date: 6 September 2018

Please cite this article as: Y. Lai, H. Su, G. Wang, X. Tang, X. Liang, X. Huang, Y. Li, H. Zhang, C. Ye, X.R. Wang, Improved microwave dielectric properties of $CaMgSi_2O_6$ ceramics through CuO doping, *Journal of Alloys and Compounds* (2018), doi: 10.1016/j.jallcom.2018.09.059.

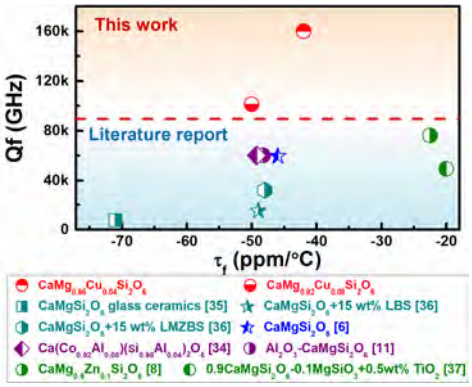

Improved microwave dielectric properties of $CaMgSi_2O_6$ ceramics through CuO doping

Yuanming Lai,[a,b] Hua Su,[a,*] Gang Wang,[a] Xiaoli Tang,[a] Xiaofeng Liang,[d] Xin Huang,[a] Yuanxun Li,[a] Huaiwu Zhang,[a] Chen Ye,[b] X. Renshaw Wang,[b,c,†]

[a] *State Key Laboratory of Electronic Thin Films and Integrated Devices, University of Electronic Science and Technology of China, Chengdu 610054, China*

b School of Physical and Mathematical Sciences, Nanyang Technological University, Singapore 637371, Singapore

[c] *School of Electrical and Electronic Engineering, Nanyang Technological University, Singapore 637371, Singapore*

[d] *Medical Institute Department, Sichuan College of Traditional Chinese Medicine, Mianyang 621000, China*

ABSTRACT: High-performance dielectric materials for microwave communication requires low dielectric constants (ε_r <10), high quality factor (*Qf*) and near-zero temperature coefficient of resonance frequency (τ_f). However, $CaMgSi_2O_6$ ceramics typically exhibit low *Qf* and largely negative τ_f, despite its low ε_r. In this study, nominal composition $CaMg_{1-x}Cu_xSi_2O_6$ ($0 \le x \le 0.16$) ceramics were synthesized via a solid-state reaction. Enhanced microwave dielectric properties were achieved in the x = 0.04 ceramics sintered at 1250 °C with ε_r = 7.41, *Qf* =160 100 GHz (two times better than the previously reported values), and τ_f = −42 ppm/°C. Benefited from the optimal CuO doping, this enhancement in microwave dielectric property was realized by the contribution of order structure and the densification. Excess CuO doping, which can lead to a phase transition (from *C2/c* to $P2_1/c$), could degenerate the microwave dielectric properties of the $CaMgSi_2O_6$ ceramics. Considering the enhanced microwave dielectric properties, the CuO-doped $CaMgSi_2O_6$ ceramic is a promising candidate material for microwave communication applications.

Keywords: $CaMgSi_2O_6$ ceramic; Microwave dielectric property; Order structure; Densification; Phase transition

* E-mail address: uestcsh77@163.com (H. Su)
† E-mail address: renshaw@ntu.edu.sg (X. Renshaw Wang)

1. Introduction

The recent rapid growth in wireless communication has led to an increasing demand for high-performance microwave dielectric materials [1,2]. In order to be applied in the wireless communications, these materials should have the low dielectric constants (ε_r < 10), high quality factor (*Qf*) and near-zero temperature coefficient of resonance frequency (τ_f) value, because the low ε_r values can shorten the delay time of signal transmission and minimize cross coupling with electrodes, high *Qf* values can decrease signal loss, and near-zero τ_f values can ensure the frequency stability as temperature changes [3–5].

$CaMgSi_2O_6$ ceramics typically exhibit a low ε_r value (~ 7.5) and is considered as an important candidate material for wireless communication devices [6–9]. However, $CaMgSi_2O_6$ ceramics possess a low *Qf* (~60 000 GHz) and largely negative τ_f (~ −46 ppm/°C), and require a high sintering temperature (1290 °C) [6]. These drawbacks directly limit the practical use of the $CaMgSi_2O_6$ ceramics. In order to improve the microwave dielectric properties, Al_2O_3, CoO and ZnO were used to dope/substitute $CaMgSi_2O_6$ ceramics [8,10,11]. However, the $CaMgSi_2O_6$–Al_2O_3, $Ca(Mg_{0.92-x}Co_xAl_{0.08})$ and $CaMg_{1-x}Zn_xSi_2O_6$ ceramics exhibited the low Qf values of ~60132, 60125 and 76100 GHz, respectively. Recently, Kuei-Chih Feng et al. [12] further investigated that Al_2O_3-doped $CaMgSi_2O_6$ glass-ceramic improved the microwave dielectric properties. The samples were sintered at low temperature of 950 °C in nitrogen atmospheres, but unfortunately the *Qf* value (~8312 GHz) was seriously deteriorated, which limits its practical application. Therefore, its relatively low *Qf* values should be improved in future studies. CuO is a promising dopant owing to its ability in improving the densification and reducing the sintering temperature [13,14]. However, there has been little study on the influence of CuO doping on the microwave dielectric properties of $CaMgSi_2O_6$ ceramic.

In this work, the nominal composition of $CaMg_{1-x}Cu_xSi_2O_6$ ($0 \le x \le 0.16$) ceramics was fabricated via a conventional solid-state process. Benefited from the low melting point of CuO, enhanced microwave properties were achieved in the CuO-doped $CaMgSi_2O_6$ ceramics. Furthermore, the influences of their structure on the microwave dielectric properties were comprehensively investigated by varying the CuO doping concentration and sintering temperature.

2. Experimental procedure

Analytically pure $CaCO_3$, MgO, CuO, and SiO_2 were used as raw materials for the nominal composition $CaMg_{1-x}Cu_xSi_2O_6$ ceramics. The raw materials were wet-mixed in a plastic container using distilled water and ZrO_2 balls. Then, the $CaMg_{1-x}Cu_xSi_2O_6$ slurries were dried and the drying mixed-powders were calcined at 1150 °C for 4 h. The calcined $CaMg_{1-x}Cu_xSi_2O_6$ powders were further milled. The mixed powders were pressed into cylindrical pellets with 12 mm in diameter and 6 mm in height and then sintered at 1100 °C–1250 °C for 4 h.

The phase composition and microstructure were analyzed through XRD (Miniflex600, Rigaku, Japan) with Cu K_α radiation, Raman scattering spectroscopy (InVia, Renishaw, UK) with an argon ion laser (λ = 514.5 nm) as the excitation light (The spectra in the range of 100–1200 cm^{-1} with a precision of ~0.3 cm^{-1} and a resolution ~1 cm^{-1}) and SEM (JSM-6490; JEOL, Japan). The microwave dielectric properties of these samples were measured through a Hakki–Coleman dielectric resonator cavity method. The changes in the resonant frequencies were obtained with a temperature of 25 and 85 °C. The τ_f (ppm/°C) values were calculated based on the following formula:

$$\tau_f = \frac{f(85℃) - f(25℃)}{60 \times f(25℃)} \times 10^6 \qquad (1)$$

3. Results and discussion

Fig. 1(a) shows the XRD patterns of the $CaMg_{1-x}Cu_xSi_2O_6$ ceramics sintered at 1200 ºC. The main phase, the monoclinic $CaMgSi_2O_6$ (ICDD no. #86-0932), was observed with increasing *x*. The secondary phases, $Ca_2MgSi_2O_7$ (ICDD no. #79-2425) and SiO_2 (ICDD no. #79-1906), were detected at x = 0. The $Ca_2MgSi_2O_7$ and SiO_2 phases disappeared, whereas the Cu_2O phase presented as the minor phase with $0.04 \leq x \leq 0.16$. The Cu_2O can be derived from CuO decomposition under high temperature as follows:

$$4CuO \rightarrow 2Cu_2O + O_2\uparrow \qquad (2)$$

The presence of Cu_2O phase could indicate that Cu^{2+} ions did not form a solid solution with $CaMgSi_2O_6$, which led to the formation of Mg-deficient $CaMgSi_2O_6$. Cu^{2+} ions can incorporate into the Mg_2SiO_4 lattice and occupy the M1 site because of the different structures between

Mg_2SiO_4 and $CaMgSi_2O_6$ [15]. The Mg_2SiO_4 crystal exhibits an orthorhombic *Pbnm* structure that consists of $M1O_6$, $M2O_6$ octahedra, and isolated SiO_4 tetrahedra. In the current study, the Ca^{2+} ions in the $CaMgSi_2O_6$ crystal occupy a distorted eightfold-coordinated M2 polyhedron (Figs. 2(a) and (b)). In addition, the Al^{3+} and Co^{2+} ions were also used to substitute Mg^{2+} ions and to form the solid solution [11,16–18]. It shall be noted that ionic substitution is related to an ionic radius and electronegativity [19,20]. In comparison to Al^{3+} (r = 0.535 Å) and Co^{2+} ions (r = 0.745 Å), the ionic radius of Cu^{2+} ions (r = 0.73 Å) is closer to that of Mg^{2+} (r = 0.72 Å). Therefore, we can conclude that the difference in the electronegativity can be more important in the formation of solid solutions of $CaMgSi_2O_6$. The back-scattering electron diffraction (BSED) and energy dispersive spectrum (EDS) of the x = 0.08 ceramics sintered at 1200 ºC are presented in Fig. 1(b). Two different kinds of black grains and white liquid morphology were observed. According to the EDS analysis, the regions of black and white contrast could correspond to $CaMgSi_2O_6$ phase and Cu_2O-rich eutectic liquid phase, respectively, which is consistent with our XRD phase evaluations and previous studies [14,21]. The parallel reactions with the x = 0 were as follows [11]:

$$CaCO_3 + MgO + 2SiO_2 \rightarrow CaMgSi_2O_6 + CO_2\uparrow \quad (3)$$

$$2CaCO_3 + MgO + 2SiO_2 \rightarrow Ca_2MgSi_2O_7 + 2CO_2\uparrow \quad (4)$$

Therefore, the $CaMgSi_2O_6$, $Ca_2MgSi_2O_7$ and SiO_2 phases were observed at x = 0 sintered at 1200 ºC. With increasing x, the reaction could occur as follows [11]:

$$Ca_2MgSi_2O_7 + MgO + 2SiO_2 \rightarrow 2CaMgSi_2O_6 \quad (5)$$

Therefore, the XRD patterns of the $Ca_2MgSi_2O_7$ and SiO_2 phases disappeared, whereas those of the $CaMgSi_2O_6$ and Cu_2O-rich eutectic liquid phase could present $0.04 \leq x \leq 0.16$. In contrast to the CuO-free $CaMgSi_2O_6$, the CuO-doping could reduce the reaction temperature (Eq. (5)) [11]. Furthermore, a new diffraction peak at 22.04° emerged as the $0.08 \leq x \leq 0.16$ (Fig. 1(a)). The appearance of the new peak indicates a phase transition from *C2/c* into $P2_1/c$ in the $CaMgSi_2O_6$ crystal due to the Mg-deficiency [22–25]. From the structure point of view, $CaMgSi_2O_6$ is a pyroxene group of minerals with a general formula of pyroxenes ($M2M1Si_2O_6$). In the holotypic structure of pyroxene diopside, Ca occupies an eightfold-coordinated M2 polyhedron (Fig. 2(b)), and Mg occupies a small and regular M1 octahedron. Both the M2 and M1 polyhedra are linked to

a SiO_4 tetrahedron [26,27]. Structurally, phase transition from *C2/c* into $P2_1/c$ is driven by the arrangement of the SiO_4 tetrahedral chain. For the $CaMgSi_2O_6$ crystal, symmetrically equivalent SiO_4 tetrahedral chains exist in *C2/c* structure, whereas two symmetrically independent SiO_4 tetrahedral chains, which have different Si–O bond lengths and deformation angles, are observed in $P2_1/c$ structure (Figs. 2(a) and 2(c)) [24,28]. The impact of the structure change on the microwave dielectric properties of these samples will be evaluated later in this study.

To study the structures of the Mg-deficient $CaMgSi_2O_6$ crystal, the XRD patterns were refined by the FullProf program [29]. The monoclinic $CaMgSi_2O_6$ with the *C2/c* space group (a = 9.7397 Å, b = 8.9174 Å, c = 5.2503 Å and β = 105.8660°) and the $P2_1/c$ space group (a = 9.7730 Å, b = 8.9620 Å, c = 5.2710 Å and β = 108.9900°) served as structure model. The refined XRD patterns with x = 0 and 0.08 and the reliability factors are presented in Fig. 3 and Table 1, respectively. The fitted patterns were consistent with the experimental data. The χ^2 factors were reasonably small. These results suggested that the refinement parameters used in the simulations were reasonable.

Fig. 4 summarizes the lattice parameters of $CaMg_{1-x}Cu_xSi_2O_6$ sintered at 1200 ºC. The refinement results showed that the lattice constant a values increased, and the b values exhibited a peak at x = 0.08 as the increasing of x value. Note that the c values decreased and β values drastic increased for x values within the range $0 \le x \le 0.08$, and then almost constant (Fig. 4). This could be due to phase transitions from *C2/c* into $P2_1/c$ at x = 0.08 [30]. The unit cell volumes firstly increased and then decreased. It is concluded that the lattice distortion induced by phase transitions.

The microstructures and morphologies of the sintered surface for $CaMg_{1-x}Cu_xSi_2O_6$ ceramics were investigated through SEM (Figs. 5(a–h)). The pores decreased and grain size increased with x increasing sintered at 1200 °C (see Figs. 5(a-d) and Figs. 6(a-d)). At $x \le 0.04$, pores and small grain (0.5–2.5 μm) were observed (see Figs. 6(a, b)). At $0.08 \le x \le 0.16$, dense microstructures were obtained because of Cu_2O-rich eutectic liquid phase, which contributed to the densification, as shown in Figs. 5(c, d) [14,31]. When sintered at 1150 ºC, pores (see Figs. 5(e,g)) and small grains (see Figs. 6 (e,g)) were observed at both x = 0.04 and 0.08, because these ceramics did not reach the optimized sintering temperatures. However, Fig. 5(h) shows that a porous

microstructure was observed at the surfaces of x = 0.08 samples sintered at a high temperature (1250 ºC), owing to the over-sintering [32]. The dense microstructure, which enhanced the microwave dielectric properties, were achieved in the $0.08 \leq x \leq 0.16$ samples sintered at 1200 ℃ and x = 0.04 sample sintered at 1250 ℃.

Raman scattering spectroscopy has been widely applied to give an insight into the crystal structure and phase transitions. Fig. 7(a) displays the Raman scattering spectroscopy of $CaMg_{1-x}Cu_xSi_2O_6$ ceramics sintered at 1200 ºC. According to the symmetry analysis of space group and Bilbao Crystallographic Server [33], the irreducible representation of optical modes for $CaMgSi_2O_6$ crystal (*C2/c* space group) could be given as follow:

$$\Gamma_{Opt} = 14A_g(R) + 16B_g(R) + 13A_u(IR) + 14B_u(IR) \quad (6)$$

The theoretical numbers of Raman and IR vibrational modes were 30 and 27, respectively. A strong Raman peak at 1011 cm^{-1} could be ascribed to the O–Si–O stretching modes [24,28,34,35]. The strong asymmetric single or double peak near 664 cm^{-1} was caused by the bending/stretching modes of the Si–O–Si bonds. The peaks at 450–600 cm^{-1} could be assigned to the O–Si–O vibrations, and the peaks at 300–450 cm^{-1} were attributed to vibration of the cations in the M1 and M2 sites that were related to tilting and chain motion of the SiO_4 tetrahedron. The Raman peaks at < 300 cm^{-1} could be assigned to the translations of the SiO_4 tetrahedron. A new peak appears at approximately 214 cm^{-1} at $x \geq 0.08$, and its intensity increases with the x increasing. This band could be due to the characteristic Raman peak of Cu_2O [36], which further verifies the Cu_2O-rich eutectic liquid phase. This finding is consistent with our XRD and EDS results. The Raman peak at ~323 cm^{-1} (A_g) shifted toward a low frequency with increasing x. This result reveals the change in the short-range order of the SiO_4 tetrahedron due to the Mg-deficiency [37]. Moreover, splitting of the 664 cm^{-1} mode at $x \geq 0.08$ was observed (Fig. 7(b)). Such splitting correlated with the structural changes that involved the silicate chains [24]. The splitting of 664 cm^{-1} peak was interpreted as the phase transition from the *C2/c* to $P2_1/c$ space group because the 664 cm^{-1} peak correlated with the bending vibration of the SiO_4 tetrahedral chain. Fig. 7(c) shows that the Raman intensities of the peak at 640 cm^{-1} increase with increasing x sintered at 1200 ℃, which indicates that the $CaMgSi_2O_6$ phase of $P2_1/c$ space group increases. This finding is consistent with the XRD results. With regard to the 320 and 664 cm^{-1} modes (Fig. 7(d)), the full width at half maximum

(FWHM) values barely changed at $x < 0.08$, but the FWHM increased as x further increased. Since FWHM values reflected the order degree [38], this result suggested that the order degree of the $CaMgSi_2O_6$ crystal gradually reduced because of the phase transition from *C2/c* to $P2_1/c$.

The ε_r values of the $CaMg_{1-x}Cu_xSi_2O_6$ ceramics with varying sintering temperatures are shown in Fig. 8(a). With the x increasing, the ε_r values increased after sintering at 1100 and 1150 ºC (Fig. 8(a)). The ε_r values initially increased and then decreased when sintered at 1200 and 1250 ºC. In general, the ε_r values of the microwave ceramics depend on the secondary phase, densification and ionic polarizability [39]. In the current study, the ε_r values were in line with the densification (Fig. 5). In addition, the Raman shift increased because of the change in polarizability in the molecule. Therefore, the relationship of the ε_r values and Raman shift could be expressed as follows [40,41]:

$$\varepsilon_r(0,\xi,k) = \frac{\Omega_P^2 exp[\lambda(E_F^0-\xi)]}{\omega(\xi,k)} \quad (7)$$

where Ω_P is the plasma frequency and ε_r and ω are the dielectric constant and phonon frequency, respectively. Based on Eq. (7), the dielectric constant is inversely proportional to the Raman shift. The ε_r values of the sintered at 1200 ºC samples and Raman shift of the phonon mode (at ~320 cm^{-1}) are shown in Fig. 8(b). When changing x, the opposite trend of the ε_r values and Raman shift of the phonon mode was observed. This agrees with the Eq. (7).

Fig. 9(a) shows the *Qf* values of the $CaMg_{1-x}Cu_xSi_2O_6$ ceramics as a function of x and sintering temperature. When fixing a sintering temperature or an x value, the *Qf* values increased initially reached the maximum and then declined with increasing x or sintering temperature. The *Qf* values are related to extrinsic losses, such as the secondary phases and densification, and also to intrinsic losses, such as the order degree and lattice vibration [42–45]. As already shown in Fig. 5, the dense microstructures were obtained with $0.08 \leq x \leq 0.16$ at 1200 °C sintering and $x = 0.04$ at 1250 °C sintering. However, the order degree gradually reduced with the x increasing because of the phase transition from *C2/c* to $P2_1/c$. Therefore, the *Qf* values of the $CaMg_{1-x}Cu_xSi_2O_6$ ceramics were in accordance with the densification and order degree. A maximum *Qf* value of 160 100 GHz was obtained for $x = 0.04$ specimens sintered at 1250 °C. Even at increased CuO content

(x = 0.08 sintered at 1200 °C), the sample presented a relatively high *Qf* value (see Figs. 9(a,b)). Comparisons of the microwave dielectric properties of $CaMgSi_2O_6$-based materials are presented in Fig. 9(b) [6,8,10,11,46–48]. The high *Qf* value could be attributed to the order structure and dense microstructure due to moderate CuO doping in this work. It can be concluded the CuO doping is an effective approach to improve the *Qf* values because it could promote the densification and do not change the structure. Fig. 9(c) shows the τ_f values as a function of x in the $CaMg_{1-x}Cu_xSi_2O_6$ ceramics. The negative τ_f values could derive from in/anti-phase tilting of the octahedra [49]. The reverse variation trend between the τ_f values and the FWHM of the Raman band is presented in Fig. 9(d), which indicated that the order structure was responsible for the stable τ_f values. The FWHM values increased with increasing x, which suggested the conversion of the structure from ordered to disordered because of the phase transition from *C2/c* to $P2_1/c$. The disordered structure can be responsible for the degeneration of the τ_f values [40].

4. Conclusions

In this work, nominal composition $CaMg_{1-x}Cu_xSi_2O_6$ ($0 \leq x \leq 0.16$) ceramics were synthesized via a solid-state route. The XRD, SEM, and EDS indicated that the Cu^{2+} ions did not form a solid solution with $CaMgSi_2O_6$. The Cu_2O-rich eutectic liquid phase located at the grain boundaries. The phase transition from *C2/c* to $P2_1/c$ was detected at $x \geq 0.08$ through XRD and Raman scattering spectroscopy. The dense microstructures were obtained with $0.08 \leq x \leq 0.16$ at 1200 °C sintering and x = 0.04 at 1250 °C sintering. Most importantly, at x = 0.04 sintered at 1250 °C, markedly improved *Qf* value of $CaMg_{1-x}Cu_xSi_2O_6$ was observed owing to order structure and densification. However, excess CuO doping, which led to phase transition because Cu^{2+} ions did not form into a solid solution with $CaMgSi_2O_6$, could degenerate the microwave dielectric properties of the $CaMgSi_2O_6$ ceramics. For the $CaMg_{1-x}Cu_xSi_2O_6$ at x = 0.04 sintered at 1250 °C for 4 h with ε_r = 7.41 and τ_f = −42 ppm/°C, the *Qf* value is 160 100 GHz, about two times higher than that reported in other literature.

Acknowledgments

This work was supported by National Natural Science Foundation of China under Grant Nos. 61771104, 61471096 and 51772047, Science and Technology Department of Sichuan Province 2016JQ0016 and 2015JQ0031, Special Projects on Science and Technology of Guizhou Province [2016]3011, National Key Research and Development Plan No. 2016YFA0300801. X.R.W. acknowledges supports from the Nanyang Assistant Professorship grant from Nanyang Technological University and Academic Research Fund Tier 1 (RG108/17S) from Singapore Ministry of Education.

References

[1] B. Ullah, W. Lei, Y. Yao, X. Wang, Structure and Synergy Performance of (1-*x*)$Sr_{0.25}Ce_{0.5}TiO_3$-*x*La($Mg_{0.5}Ti_{0.5}$)O_3 based microwave dielectric ceramics for 5G architecture architecture, J. Alloys Compd. 763 (2018) 990–996.

[2] D. Zhou, L. Pang, D. Wang, Z. Qi, I.M. Reaney, High Quality Factor, Ultralow sintering temperature $Li_6B_4O_9$ microwave dielectric ceramics with ultralow density for antenna substrates, ACS Sustain. Chem. Eng. 6 (2018) 11138–11143.

[3] B.K. Choi, S.W. Jang, E.S. Kim, Dependence of microwave dielectric properties on crystallization behaviour of $CaMgSi_2O_6$ glass-ceramics, Mater. Res. Bull. 67 (2015) 234–238.

[4] Y. Guo, J. Ma, J. Zhao, K. Du, Z. Fang, Y. Zheng, W.-Z. Lu, W. Lei, Low-temperature sintering and microwave dielectric properties of $CaSn_xSiO_{(3+2x)}$-based positive τf compensator, Ceram. Int. 44 (2018) 18209–18212.

[5] X.-Q. Song, K. Du, X.-Z. Zhang, J. Li, W.-Z. Lu, X.-C. Wang, W. Lei, Crystal structure , phase composition and microwave dielectric properties of $Ca_3MSi_2O_9$ ceramics, J. Alloys Compd. 750 (2018) 996–1002.

[6] H. Sun, Q. Zhang, H. Yang, J. Zou, $(Ca_{1-x}Mg_x)SiO_3$: A low-permittivity microwave dielectric ceramic system, Mater. Sci. Eng. B Solid-State Mater. Adv. Technol. 138 (2007) 46–50.

[7] Q.L. Zhang, H. Yang, H.P. Sun, A new microwave ceramic with low-permittivity for LTCC applications, J. Eur. Ceram. Soc. 28 (2008) 605–609.

[8] J. Zhang, Y. Zhou, Z. Yue, Low-temperature sintering and microwave dielectric properties of LiF-doped $CaMg_{1-x}Zn_xSi_2O_6$ ceramics, Ceram. Int. 39 (2013) 2051–2058.

[9] C.C. Chou, C.Y. Chang, G.Y. Chen, W.J. Liao, K.C. Feng, C.Y. Tsao, Control of silver diffusion in low-temperature co-fired diopside glass-ceramic microwave dielectrics, Materials (Basel). 11 (2017) 1–9.

[10] D. Li, H. Wang, Y. Tang, Q. Yang, R. Lei, Effect of Co^{2+} substitution on sintering behavior and microwave ceramics, J. Ceram. Soc. Japan. 123 (2015) 1080–1083.

[11] H. Wang, D. Li, Q. Yang, R. Lei, H. Ma, S. Xu, Sintering behavior and microwave dielectric properties of $CaMgSi_2O_6$ ceramics with Al_2O_3 addition, Mater. Res. Bull. 54 (2014) 66–72.

[12] K. Feng, P. Chen, P. Wu, C. Chen, C. Tu, Reducing-atmosphere resistant mechanism on microwave dielectric enhancement of $CaMgSi_2O_6$ glass-ceramics, J. Alloys Compd. 765 (2018) 75–81.

[13] L. Cheng, L. Liu, Q. Ma, S. Liu, Relationship between densification behavior and stabilization of quasi-liquid grain boundary layers in CuO-doped $0.7CaTiO_3$–$0.3NdAlO_3$ microwave ceramics, Scr. Mater. 111 (2016) 102–105.

[14] J. Nie, J.M. Chan, M. Qin, N. Zhou, J. Luo, Liquid-like grain boundary complexion and sub-eutectic activated sintering in CuO-doped TiO_2, Acta Mater. 130 (2017) 329–338.

[15] Y. Lai, X. Tang, X. Huang, H. Zhang, X. Liang, J. Li, H. Su, Phase composition, crystal structure and microwave dielectric properties of $Mg_{2-x}Cu_xSiO_4$ ceramics, J. Eur. Ceram. Soc. 38 (2018) 1508–1516.

[16] H. Wang, D. Li, Q. Yang, R. Lei, H. Ma, S. Xu, Sintering behavior and microwave dielectric properties of a new low-permittivity ceramic system $Ca(Mg_{1-x}Al_x)(Si_{1-x/2}Al_{x/2})_2O_6$, Ceram. Int. 40 (2014) 3333–3339.

[17] C.G.M. Tribaudino, F.M.H. Skogby, Co^{2+}-doped diopside: crystal structure and optical properties, Phys. Chem. Miner. 45 (2018) 443–461.

[18] D. Delmonte, C. Gori, E. Lambruschi, A comprehensive study of the magnetic properties of the pyroxenes series $CaMgSi_2O_6$-$Co_2Si_2O_6$ as a function of Co content, J. Phys. Condens. Matter. 30 (2018) 285801.

[19] H. Chen, H. Su, H. Zhang, T. Zhou, B. Zhang, J. Zhang, X. Tang, Low-temperature sintering and microwave dielectric properties of $(Zn_{1-x}Co_x)_2SiO_4$ ceramics, Ceram. Int. 40 (2014) 14655–14659.

[20] Y. Zhao, P. Zhang, Influence of Ta substitution for Nb in $Zn_3Nb_2O_8$ and the impact on the crystal structure and microwave dielectric properties, Dalt. Trans. 45 (2016) 11807–11816.

[21] C. Hsu, C. Huang, J. Tseng, Improved high-Q microwave dielectric resonator using CuO-doped $MgNb_2O_6$ ceramics, Mater. Res. Bull. 38 (2003) 1091–1099.

[22] M. Tribaudino, High-pressure behaviour of Ca-rich C2/c→P21/c clinopyroxenes along the join diopside-enstatite ($CaMgSi_2O_6$-$Mg_2Si_2O_6$) join, Am. Mineral. 85 (2000) 707–715.

[23] M. Tribaudino, M. Prencipe, M. Bruno, D. Levy, High-pressure behaviour of Ca-rich C2/c clinopyroxenes along the join diopside-enstatite, Phys. Chem. Miner. 27 (2000) 656–664.

[24] M. Tribaudino, L. Mantovani, D. Bersani, P.P. Lottici, Raman spectroscopy of (Ca,Mg)$MgSi_2O_6$ clinopyroxenes, Am. Mineral. 97 (2012) 1339–1347.

[25] M. Tribaudino, L. Mantovani, F. Mezzadri, G. Calestani, G. Bromiley, the C2/c-P21/c phase transition in natural and synthetic Ca-Mg-Fe^{2+} pyroxenes, Mineral. J. 82 (2018) 211–228.

[26] L. Mantovani, M. Tribaudino, F. Mezzadri, G. Calestani, G. Bromiley, The structure of (Ca,Co)$CoSi_2O_6$ pyroxenes and the Ca-M^{2+} substitution in (Ca,M^{2+})$M^{2+}Si_2O_6$ pyroxenes (M^{2+} = Co, Fe, Mg), Am. Mineral. 98 (2013) 1241–1252.

[27] F. Nestola, A. Madsen, M. Tribaudino, T. Balić Žunić, H. Ohashi, L. Secco, A.D. Negro, Low-temperature crystal structure evolution of (Na,Ca)(Cr,Mg)Si_2O_6 pyroxene, Mineral. Mag. 72 (2008) 809–816.

[28] L. Mantovani, M. Tribaudino, I. Aliatis, E. Lambruschi, P.P. Lottici, D. Bersani, Raman spectroscopy of $CaCoSi_2O_6$-$Co_2Si_2O_6$ clinopyroxenes, Phys. Chem. Miner. 42 (2015) 179–189.

[29] J. Rodríguez-Carvajal, Recent advances in magnetic structure determination by neutron powder diffraction, Phys. B Condens. Matter. 192 (1993) 55–69.

[30] R.C. Newton, T. V. Charlu, P.A.M. Anderson, O.J. Kleppa, Thermochemistry of synthetic clinopyroxenes on the join $CaMgSi_2O_6$-$Mg_2Si_2O_6$, Geochim. Cosmochim. Acta. 43 (1979) 55–60.

[31] S.Q. Yu, B. Tang, X. Zhang, S.R. Zhang, X.H. Zhou, Improved high-Q microwave dielectric ceramics in CuO-doped $BaTi_4O_9$-$BaZn_2Ti_4O_{11}$ system, J. Am. Ceram. Soc. 95 (2012) 1939–1943.

[32] B. Zhang, L. Li, Microstructure and microwave dielectric properties of CuO-modified $CoWO_4$ ceramics, J. Mater. Sci. Mater. Electron. 28 (2017) 3523–3529.

[33] E. Kroumova, M.I. Aroyo, J.M. Perez-Mato, A. Kirov, C. Capillas, S. Ivantchev, H. Wondratschek, Bilbao crystallographic server : useful databases and tools for phase-transition studies, Phase Transitions. 76 (2003) 155–170.

[34] M. Tribaudino, I. Aliatis, D. Bersani, G.D. Gatta, E. Lambruschi, L. Mantovani, G. Redhammer, P.P. Lottici, High-pressure Raman spectroscopy of Ca(Mg,Co)Si_2O_6 and Ca(Mg,Co)Ge_2O_6 clinopyroxenes, J. Raman Spectrosc. 48 (2017) 1443–1448.

[35] E. Lambruschi, I. Aliatis, L. Mantovani, M. Tribaudino, D. Bersani, G.J. Redhammer, P.P. Lottici, Raman spectroscopy of $CaM^{2+}Ge_2O_6$ (M^{2+} = Mg, Mn, Fe, Co, Ni, Zn) clinopyroxenes, J. Raman Spectrosc. 46 (2015) 586–590.

[36] Y. Deng, A.D. Handoko, Y. Du, S. Xi, B.S. Yeo, In situ Raman spectroscopy of copper and copper oxide surfaces during electrochemical oxygen evolution reaction : identification of Cu III oxides as catalytically active species, ACS Catal. 6 (2016) 2473–2481.

[37] S.D. Ramarao, V.R.K. Murthy, Structural, Raman spectroscopic and microwave dielectric studies on spinel $Li_2Zn_{(1-x)}Ni_xTi_3O_8$ compounds, Dalt. Trans. 44 (2015) 2311–2324. [38] Y. Wang, L. Hu, Q. Zhang,

H. Yang, Phase transition characteristics and associated piezoelectricity of potassium-sodium niobate lead-free ceramics, Dalt. Trans. 44 (2015) 13688–13699.

[39] S.D. Ramarao, V.R.K. Murthy, Crystal structure refinement and microwave dielectric properties of new low dielectric loss $AZrNb_2O_8$ (A: Mn, Zn, Mg and Co) ceramics, Scr. Mater. 69 (2013) 274–277.

[40] F. Shi, H. Dong, Correlation of crystal structure, dielectric properties and lattice vibration spectra of $(Ba_{(1-x)}Sr_{(x)})(Zn_{(1/3)}Nb_{(2/3)})O_3$ solid solutions., Dalton Trans. 40 (2011) 6659–67. [41]A. Das Arulsamy, Renormalization group method based on the ionization energy theory, Ann. Phys. (N. Y). 326 (2011) 541–565.

[42] C. Zhang, R. Zuo, J. Zhang, Y. Wang, Structure-dependent microwave dielectric properties and middle-temperature sintering of forsterite $(Mg_{1-x}Ni_x)_2SiO_4$ ceramics, J. Am. Ceram. Soc. 98 (2015) 702–710. [43] J. Zhang, J. Zhai, X. Chou, J. Shao, X. Lu, X. Yao, Microwave and infrared dielectric response of tunable $Ba_{1-x}Sr_xTiO_3$ ceramics, Acta Mater. 57 (2009) 4491–4499. [44] P. Zhang, Y. Zhao, W. Haitao, Bond ionicity, lattice energy, bond energy and microwave dielectric properties of $ZnZr(Nb_{1-x}A_x)_2O_8$ (A = Ta, Sb) ceramics, Dalt. Trans. 44 (2015) 16684–16693.

[45] S. George, M.T. Sebastian, Synthesis and microwave dielectric properties of novel temperature stable high Q, $Li_2ATi_3O_8$ (A=Mg, Zn) ceramics, J. Am. Ceram. Soc. 93 (2010) 2164–2166.

[46] K.C. Feng, C. Lin, C.C. Chou, L. Chu, Effect of particle size on crystallization and microwave dielectric characteristics of $CaMgSi_2O_6$ glass-ceramics, Ferroelectrics. 435 (2012) 91–97.

[47] T. Joseph, M.T. Sebastian, Effect of glass addition on the microwave dielectric properties of $CaMgSi_2O_6$ ceramics, Int. J. Appl. Ceram. Technol. 7 (2010) E98–E106.

[48] Y.J. Eoh, E.S. Kim, Effect of heat-treatment on the dielectric properties of $CaMgSi_2O_6$ glass-ceramics with Cr_2O_3–Fe_2O_3–TiO_2, Jpn. J. Appl. Phys. 53 (2014) 08NB01-5.

[49] G.S. Babu, V. Subramanian, V.R.K. Murthy, I.-N. Lin, C.-T. Chia, H.-L. Liu, Far-infrared, Raman spectroscopy, and microwave dielectric properties of $La(Mg_{0.5}Ti_{(0.5-x)}Sn_x)O_3$ ceramics, J. Appl. Phys. 102 (2007) 064906.

Figure captions:

Fig. 1. XRD and BSED results of $CaMg_{1-x}Cu_xSi_2O_6$ ceramics. (a) The XRD patterns of the $CaMg_{1-x}Cu_xSi_2O_6$ ceramics sintered at 1200 ºC; (b) BSED of the x = 0.08 ceramics sintered at 1200 ºC (The associated energy dispersive X-ray spectrum is inserted).

Fig. 2. $CaMgSi_2O_6$ crystal structure with different phase and Ca-cluster (a) The *C2/c* structure patterns, (b) The cluster of eightfold coordinated Ca polyhedron, (c) The $P2_1/c$ structure patterns.

Fig. 3. Refined XRD pattern for $CaMg_{1-x}Cu_xSi_2O_6$ sintered at 1200 ºC, (a) x = 0, (b) x = 0.08, showing the calculated and experimental profile.

Fig. 4. The cell parameters of $CaMg_{1-x}Cu_xSi_2O_6$ sintered at 1200 ºC.

Fig. 5. SEM images of $CaMg_{1-x}Cu_xSi_2O_6$ ceramics.

Fig. 6. The grain size distribution of $CaMg_{1-x}Cu_xSi_2O_6$ ceramics.

Fig.7. (a) Raman scattering spectroscopy of $CaMg_{1-x}Cu_xSi_2O_6$ ceramics sintered at 1200 ºC; (b) Raman fit of x = 0.04 and x = 0.08 sample; (c) Raman intensity of 640 cm^{-1}; (d) FWHM of Raman peaks at 320 and 664 cm^{-1}.

Fig. 8. (a) The ε_r values of the $CaMg_{1-x}Cu_xSi_2O_6$ ceramics with different sintering temperature; (b) The ε_r values of the ceramics sintered at 1200 ºC versus Raman shift.

Fig. 9. Microwave properties of $CaMg_{1-x}Cu_xSi_2O_6$ ceramics. (a) The Qf values of the $CaMg_{1-x}Cu_xSi_2O_6$ ceramics; (b) Summary of Qf and τ_f values of various $CaMgSi_2O_6$ from different works; (c) τ_f values of the $CaMg_{1-x}Cu_xSi_2O_6$ ceramics; (d) The τ_f values of the ceramics sintered at 1200 ºC versus FWHM.

Table captions:

Table 1. The reliability factors from Rietveld refinement for $CaMg_{1-x}Cu_xSi_2O_6$ ceramics.

Table 1. The reliability factors from Rietveld refinement for $CaMg_{1-x}Cu_xSi_2O_6$ ceramics.

Reliability factors \ x	0	0.04	0.08	0.12	0.16
R_p (%)	11.00	9.54	10.70	12.60	16.00
R_{wp} (%)	14.20	10.30	11.10	13.20	16.80
R_{exp} (%)	9.40	10.11	10.51	10.95	11.13
χ^2	2.28	1.04	1.12	1.46	2.28

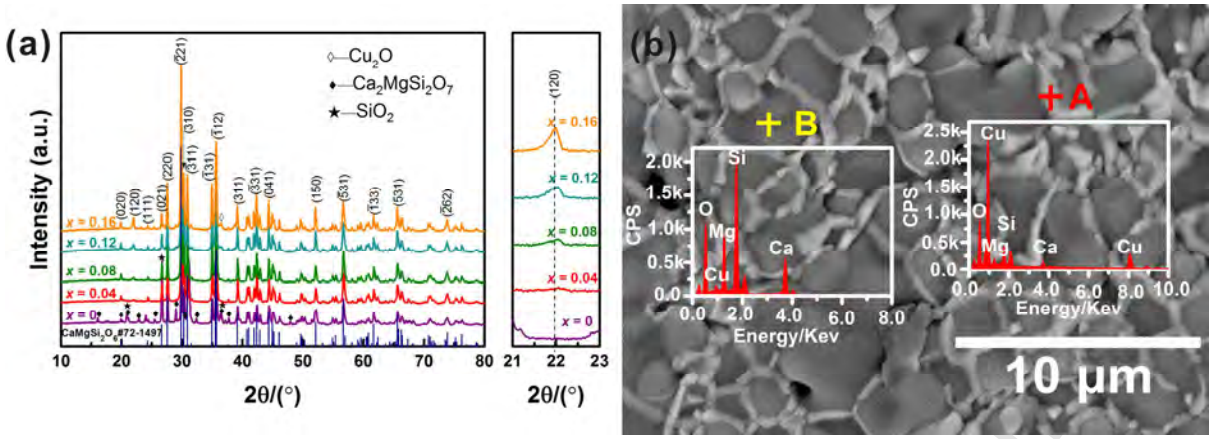

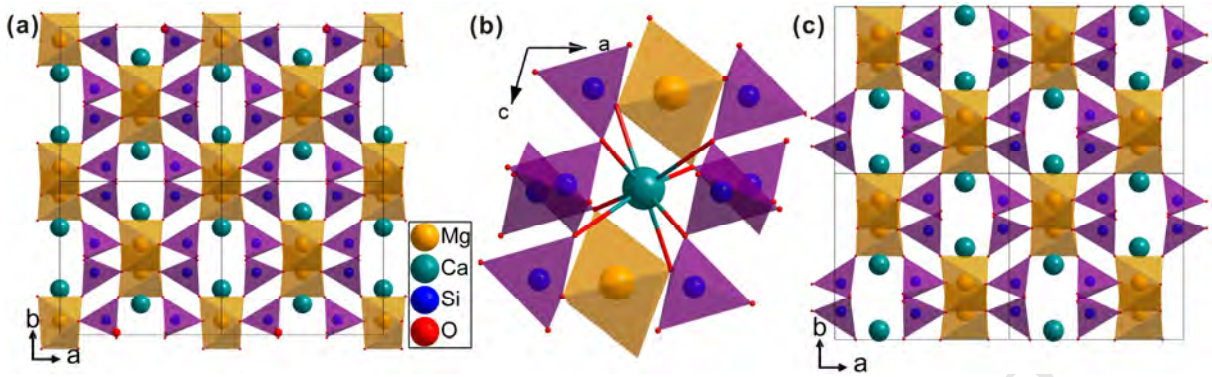

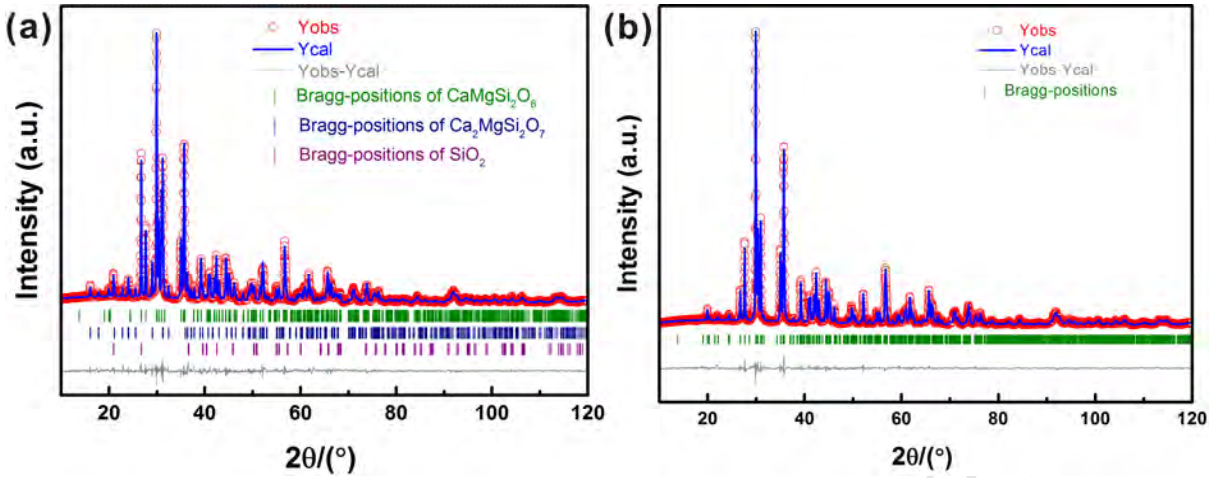

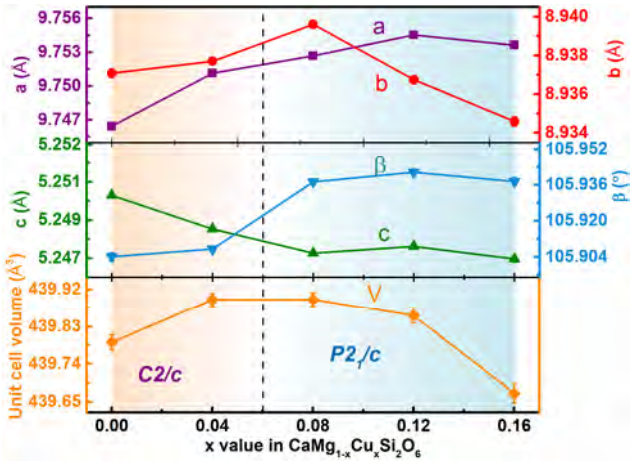

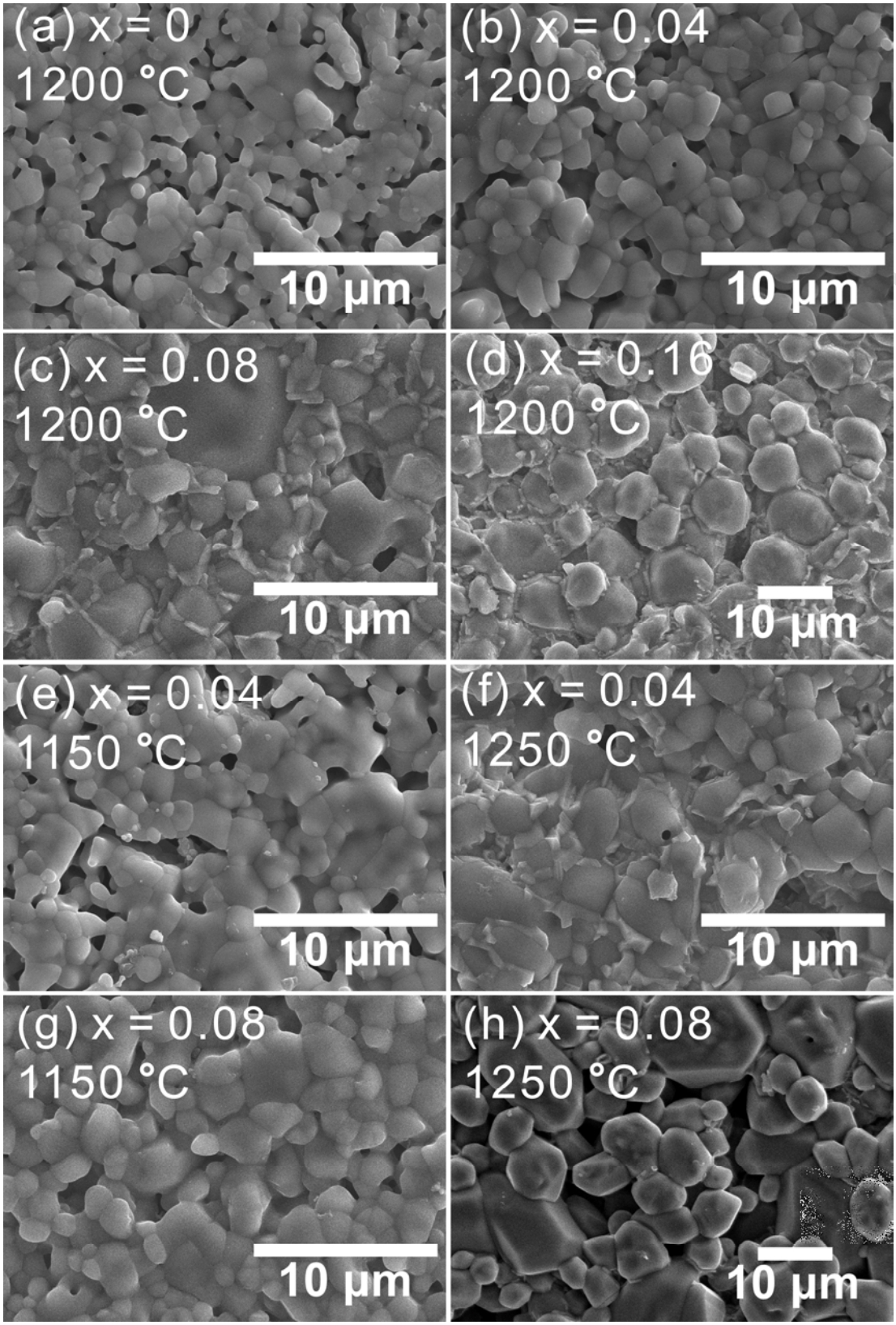
(a) x = 0
1200 °C
10 µm
(b) x = 0.04
1200 °C
10 µm
(c) x = 0.08
1200 °C
10 µm
(d) x = 0.16
1200 °C
10 µm
(e) x = 0.04
1150 °C
10 µm
(f) x = 0.04
1250 °C
10 µm
(g) x = 0.08
1150 °C
10 µm
(h) x = 0.08
1250 °C
10 µm

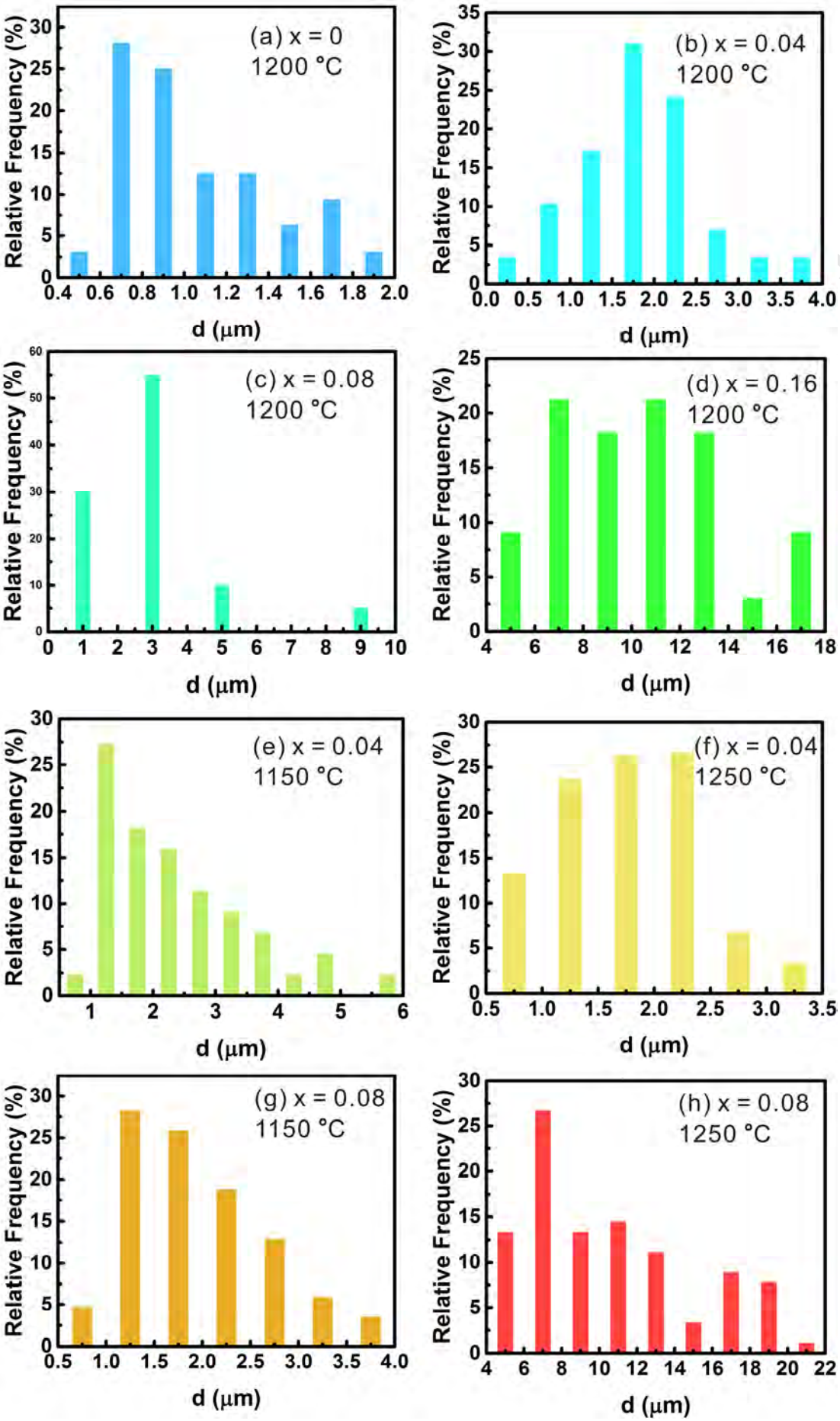
(a) x = 0
1200 °C
(b) x = 0.04
1200 °C
(c) x = 0.08
1200 °C
(d) x = 0.16
1200 °C
(e) x = 0.04
1150 °C
(f) x = 0.04
1250 °C
(g) x = 0.08
1150 °C
(h) x = 0.08
1250 °C
Relative Frequency (%)
d (μm)

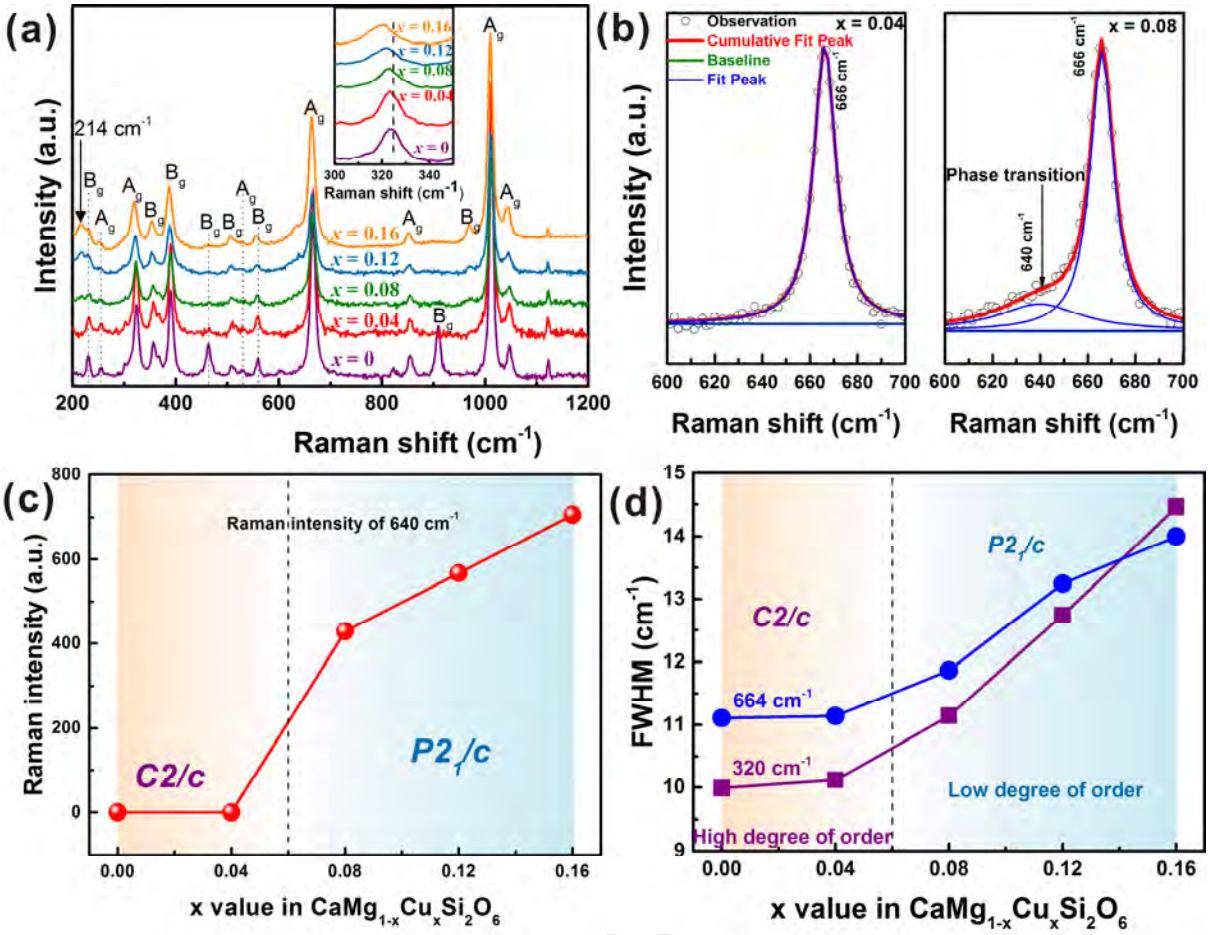

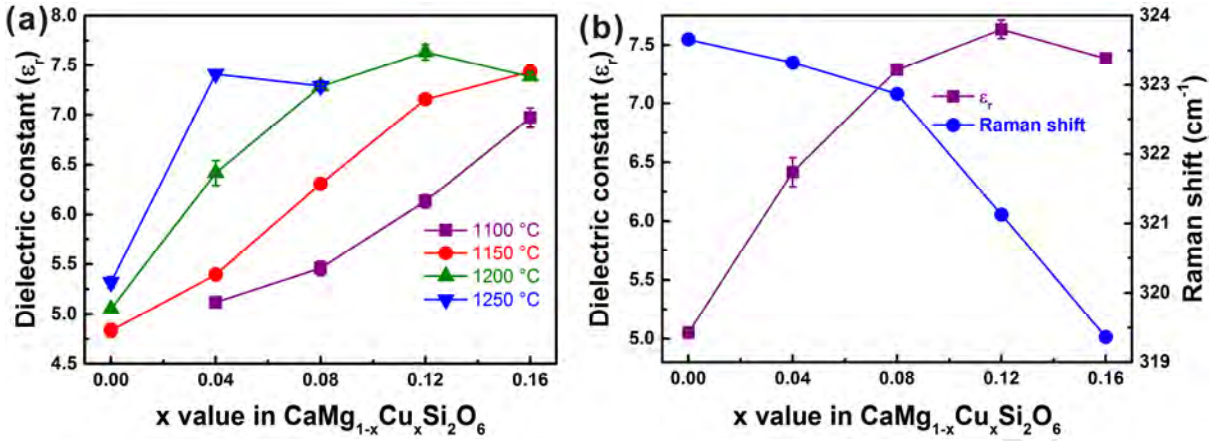

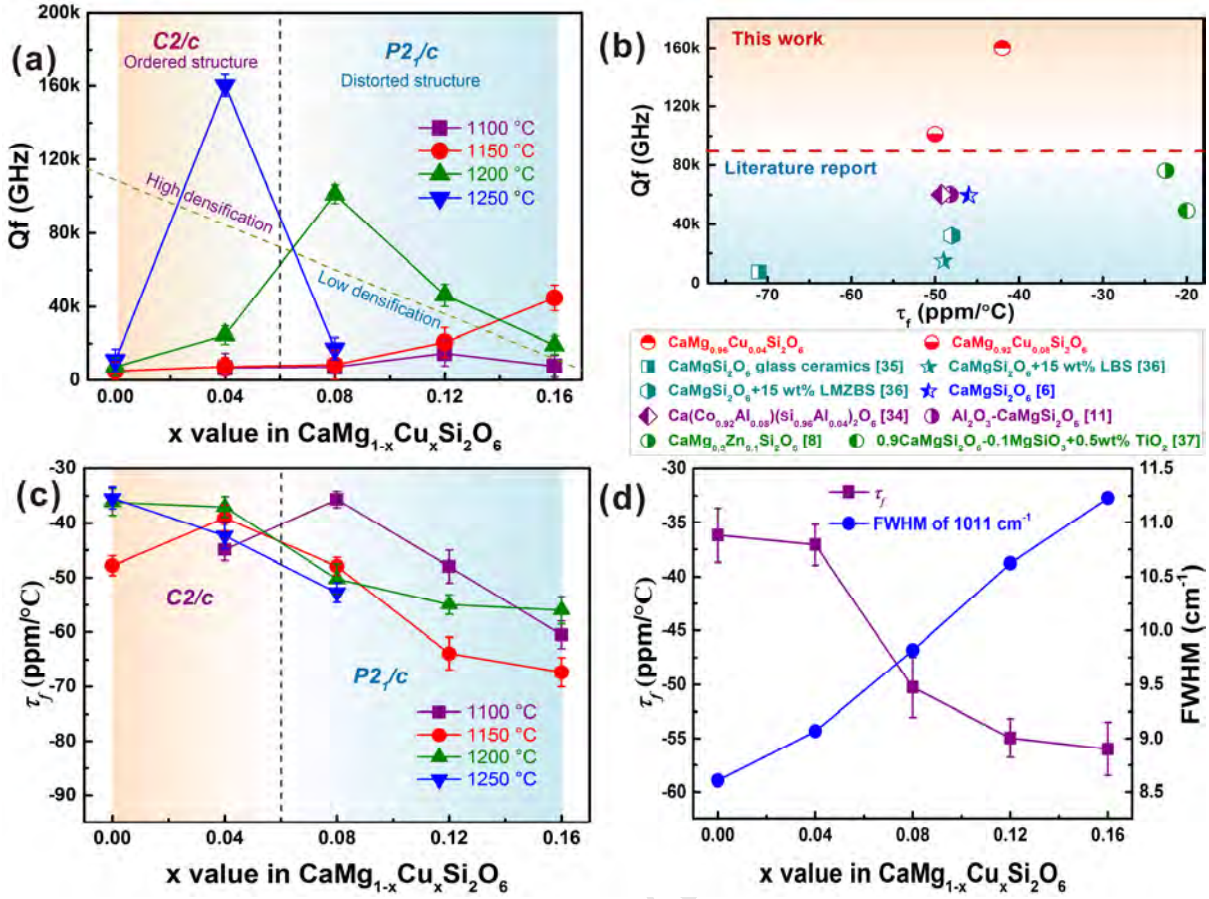

Highlights

1. Enhanced dielectric properties of $CaMgSi_2O_6$ were realized by moderate CuO doping.

2. The maximum Qf of CuO-doped $CaMgSi_2O_6$ is ~two times higher than previously reported.

3. Mg defect can lead to phase transition of $CaMgSi_2O_6$ from *C2/c* to $P2_1/c$.

4. Excess CuO doping could degenerate the microwave dielectric properties.